Ground-penetrating radar mapping of Minoan volcanic deposits and the Late Bronze Age palaeotopography, Thera, Greece

JAMES K. RUSSELL[1] & MARK V. STASIUK[2]

[1] *Igneous Petrology Laboratory, Department of Earth and Ocean Sciences, University of British Columbia, Vancouver, B.C. V6T 1Z4, Canada (e-mail: russell@perseus.geology.ubc.ca)*

[2] *Environmental Science Division, Institute of Environmental and Biological Sciences, Lancaster University, Lancaster LA1 4YQ, UK*

Abstract: The Late Bronze Age (LBA) eruption of Santorini volcano deposited ash over most of the eastern Mediterranean, distributed thick deposits of pyroclastic material over the local landscape, and instantly buried the Minoan-aged living surface of these islands. Ground-penetrating radar (GPR) studies of the LBA volcanic deposits on Thera have allowed us to establish the thickness of individual pyroclastic units, to trace units laterally, and to establish facies variations in areas where the deposits are unexposed. GPR data are presented for two sites: Site A is a survey over LBA volcanic deposits exposed in the Phira quarry, immediately south of the town of Phira, and Site B is a 550 m survey of the LBA deposits underlying the Akrotiri peninsula immediately north and south of the Akrotiri archaeological excavation. These traverses show that GPR can define structures as deep as 18–20 m (velocity 0.1 m ns^{-1}) and can accurately map the thicknesses of the LBA volcanic deposits from the caldera wall to Thera's southern coast. Furthermore, our best datasets suggest that the Phase 1 fall deposits can be differentiated from the Phase 2–4 deposits, and that GPR can clearly image the interface between the volcanic deposits and the underlying LBA living surface. Future GPR surveys could be used to delineate palaeotopographic lows and valleys associated with LBA streams or drainages or, used in combination with geological mapping, could refine the position and nature of LBA shorelines.

The present-day landscape of the Santorini islands results directly from the Late Bronze Age (LBA) or Minoan eruption of Santorini volcano. The eruption enlarged the central caldera to its present 70–80 km^2 and produced a series of rhyodacitic pyroclastic deposits that blanket most of the islands (Bond & Sparks 1976; Heiken & McCoy 1984; Druitt 1990). The deposits bury the Minoan living surface to depths of tens of metres; in several instances, the pyroclastic deposits have buried several important Minoan settlements (e.g. Marinatos 1939; Sparks 1979; McCoy & Heiken 1994), the most notable of which is that near Akrotiri on the south coast of Thera.

In this paper we explore the potential of ground-penetrating radar (GPR) for subsurface mapping of the LBA pyroclastic deposits on Thera. GPR data are presented for two sites (Fig. 1). Site A is a calibration survey over LBA volcanic deposits exposed in the Phira quarry, immediately south of the town of Phira, and Site B is a regional 550 m survey of the LBA deposits underlying the Akrotiri peninsula immediately north and south of the Akrotiri archaeological excavation. Our original intent was to use GPR to map volcanic stratigraphy. Specifically, we aimed to map volcanic deposits in regions that had little vertical exposure and to trace individual pyroclastic units within the subsurface. This endeavour is relevant in that the Minoan deposits are relatively undissected and, except along the crater wall or the coastlines, are poorly exposed. Stratigraphic measurements such as these can provide hard data with which to constrain ideas on the eruptive and depositional processes attending the LBA eruption.

Our results also directly benefit archaeological investigations. With GPR, we are clearly able to image the interface between the LBA volcanic deposits and the underlying Minoan living surface (e.g. Vaughan 1986; McCoy *et al.* 1992; Camerlynck *et al.* 1994; Goodman 1994). Radar surveys, therefore, can show the total thickness

From: McGuire, W. G., Griffiths, D. R., Hancock, P. L. & Stewart, I. S. (eds) *The Archaeology of Geological Catastrophes*. Geological Society, London, Special Publications, **171**, 105–121. 1-86239-062-2/00/ $15.00

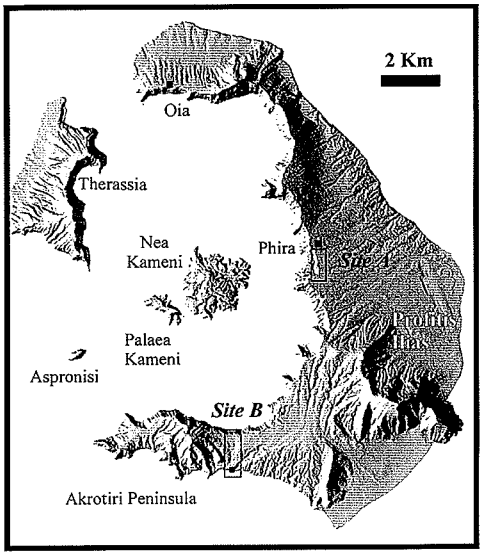

Fig. 1. Physiographic map of Santorini showing the locations of surveys in relation to major geographical features. Survey sites include the Phira quarry (Site A) and a traverse across the Akrotiri peninsula (Site B). Digital elevation model cartography is courtesy of Tim Druitt.

of volcanic material overlying specific sites or horizons, can map palaeotopography in the subsurface, and can map the position and nature of the ancient Minoan shorelines (e.g. Heiken *et al.* 1990; Druitt & Francaviglia 1992; Forsyth 1996; Friedrich *et al.* 2000).

The Minoan volcanic deposits

The Santorini islands include Thera, Therassia, Aspronisi and the younger Palaea Kameni and Nea Kameni (Fig. 1). Thera, Therassia and Aspronisi are remnants of the LBA island that was partially destroyed and heavily modified by the cataclysmic 3600 years BP (e.g. Aitken 1988) Plinian eruption of Santorini volcano. These islands form a broken ring around the now-flooded caldera, produced by a series of collapse events associated with the Minoan and previous voluminous eruptions (Heiken & McCoy 1984; Druitt & Francaviglia 1992; Forsyth 1996). The Kameni islands are substantially younger than the LBA eruption (e.g. Fytikas *et al.* 1990) and are, in fact, the emergent portions of a large ($2\,km^3$) submarine dacitic intracaldera shield volcano. There have been at least nine subaerial eruptions between 197 BC and 1950 (Fytikas *et al.* 1990; Druitt *et al.* 1996).

The Minoan eruption of Santorini produced over $36\,km^3$ of volcanic material. Previous workers have established a stratigraphy of four mappable pyroclastic units (Phases 1–4). Below is a summary of the eruption sequence and a description of the resulting pyroclastic deposits based on the work of Bond & Sparks (1976), Heiken & McCoy (1984) and Druitt (1990), and summarized by Druitt *et al.* (1999). The eruption began with phreatic and phreatomagmatic explosions from a vent near present-day Nea Kameni and showered SE Thera with about $10^6\,m^3$ of ash (Heiken & McCoy 1984; Doumas *et al.* 1997). The Plinian phase of the main eruption (Phase 1) commenced at the same vent and the column attained a height of 36 km (Sigurdsson *et al.* 1990). Phase 1 fall deposits represent *c.* $2\,km^3$ of magma and occur over all of the Santorini islands to a maximum depth of 6 m. Several hours into the Plinian eruption, sea water gained access to the vent, causing violent phreatomagmatic explosions and the production of surge deposits (Phase 2). The surge deposits are laminated, cross-bedded and poorly sorted, and are themselves overlain by massive, poorly sorted deposits up to 35 m thick (Phase 3). The Phase 3 deposits are thought to represent low-temperature, fluid-rich pyroclastic flows caused by high-intensity phreatomagmatic explosions. Phase 4 deposits are dominantly fine-grained ignimbrite and are thought to derive from high-temperature pyroclastic flows; they are distributed mainly around the outer coasts of Thera, Therassia and Aspronisi. The Phase 4 deposits are fan-shaped in cross-section, in that they thicken with distance from the caldera wall (up to 40 m). One of the most notable features of the Phase 4 deposits is the abundance of lenses and layers of lithic breccias enclosed within the fine-grained ignimbrite. Lastly, overlying the entire eruption sequence, there are alluvial deposits associated with flash floods presumed to have occurred shortly after the Plinian eruption. In the vicinity of the Akrotiri excavation site, these alluvial gravel and boulder deposits have eroded and covered the Phase 4 ignimbrite.

Ground-penetrating radar

GPR is used extensively for imaging the shallow subsurface; the technique uses electromagnetic (EM) waves in the Megahertz (MHz) frequency range to image subsurface variations in electrical properties. Conceptually, it is the EM analogue of reflection seismology (e.g. Ardon 1985); the fundamental principles of the technique have been well described by Annan & Davis (1977) and Davis & Annan (1989).

GPR has been used effectively in the fields of glaciology (e.g. Clarke & Cross 1989), geotechnical engineering (e.g. Ardon 1985; Holloway *et al.* 1986), environmental geophysics (Knoll *et al.* 1991; Rea *et al.* 1994) and, recently, in archaeology (e.g. Vaughan 1986; Goodman 1994; Camerlynck *et al.* 1994; Marco *et al.* 1997) as a complement to other geophysical surveys (e.g. Williams & Cronkite-Price 1995). The development of higher-power transmitters (e.g. 1000 V), lower-frequency antennae (e.g. <50 MHz) and more focused beams has improved the effectiveness of the technique for geological studies. For example, GPR has been used on a wide variety of lithified geological deposits such as clastic sedimentary rocks (e.g. Jol & Smith 1992; Smith & Jol 1992), Palaeozoic limestone reefs (Pratt & Miall 1993), and more structurally complex rocks (e.g. Holloway *et al.* 1986; Liner & Liner 1995).

Volcanic stratigraphy is particularly appropriate for study by GPR because the deposits are commonly thin and compositionally homogeneous, and they can be electrically resistive (Stasiuk & Russell 1994; Russell & Stasiuk 1997). The deposits on Thera are also particularly dry and situated well above the water table, which means that there will be little attenuation of the radar signal by pore or surface water. Previous studies by McCoy *et al.* (1992), Stasiuk & Russell (1994), Gilbert *et al.* (1996), Russell & Stasiuk (1997) and Russell *et al.* (1998) have shown that GPR has tremendous potential for quantifying distributions, thicknesses and volumes of volcanic deposits, and perhaps can even be used to study facies variations within individual units.

Radar survey conditions

All GPR data were collected with a Sensors and Software 'PulseEKKO' 100 instrument. The radar was controlled with a Toshiba 486 PC laptop. During the course of the field programme we experimented with different configurations of antennae (50 and 100 MHz) and transmitters (400 and 1000 V). On the basis of these experiments, we elected to use a 1000 V source and the 50 MHz antennae for our surveys. Transmitter and console computer were powered by a rechargeable, 13 A, 12 V gelsel battery.

Table 1 summarizes the survey variables (e.g. acquisition time windows, etc.) for all traverses presented in this paper. Apart from a single common-mid-point (CMP) survey, all surveys were run in common-offset reflection mode. We employed a 3 m separation between transmitter and receiver antennae to reduce the effects of ringing on surveys with longer listening times (e.g. MK4A). Data were collected with a fixed gain but, for interpretation and presentation purposes, were analysed with automatic gain control (AGC) or spreading and exponential compensation (SEC) gain control. Both gain functions are standard options within the PulseEKKO 4.2 software. Gain artificially increases the amplitudes of signals recorded in the traces and can be used to visually compensate for decreased amplitudes reflected from greater depths. Increasing gain to elucidate deeper structures is effective only where reflected amplitudes are significantly larger than background noise amplitudes (large signal to noise ratio).

Situated at the top of Mount Profitis Ilias (Fig. 1) is a large radar installation that appears to serve civilian and military air traffic control. The installation has line-of-sight over most of Thera and broadcasts a signal continuously. This signal was received by our antenna with the result that each trace contains two components of energy: (a) the portion of our original EM pulse that was reflected from subsurface features, and (b) energy derived from the ambient cultural radar. The second component contributes high-frequency noise to each trace. For shallow reflectors this noise represents little more than a nuisance because the signal (primary reflection) to noise (ambient cultural radar) ratio is high.

Table 1. *Survey variables used for each traverse segment, including listening time (TW), stacking, number of traces collected and sample interval (SI)*

Site	Location	Mode	Files	TW (ns)	Stacks	Traces	SI (m)	Length (m)
A	Phira quarry	CMP	CMP1	512	64	54	0.2	–
A	Phira quarry	COR	MK1E	512	256	283	0.5	141
B	Akrotiri	COR	MK4A	900	256	80	1.0	79
B	Akrotiri	COR	MK4B	512	128	200	1.0	199
B	Akrotiri	COR	MK4C	512	128	160	1.0	159
B	Akrotiri	COR	MK4D	512	128	192	1.0	191

CMP, common-mid-point survey; COR, common-offset reflection survey.

For deeper reflectors, however, our ability to image is severely impeded because primary signals generally become weaker with depth, resulting in a low signal to noise ratio. In such instances, gain cannot be used to enhance the primary signals without increasing the noise. We found that when we operated within line-of-sight of Profitis Ilias the background radar signal masked all reflectors at depths greater than *c.* 8 m.

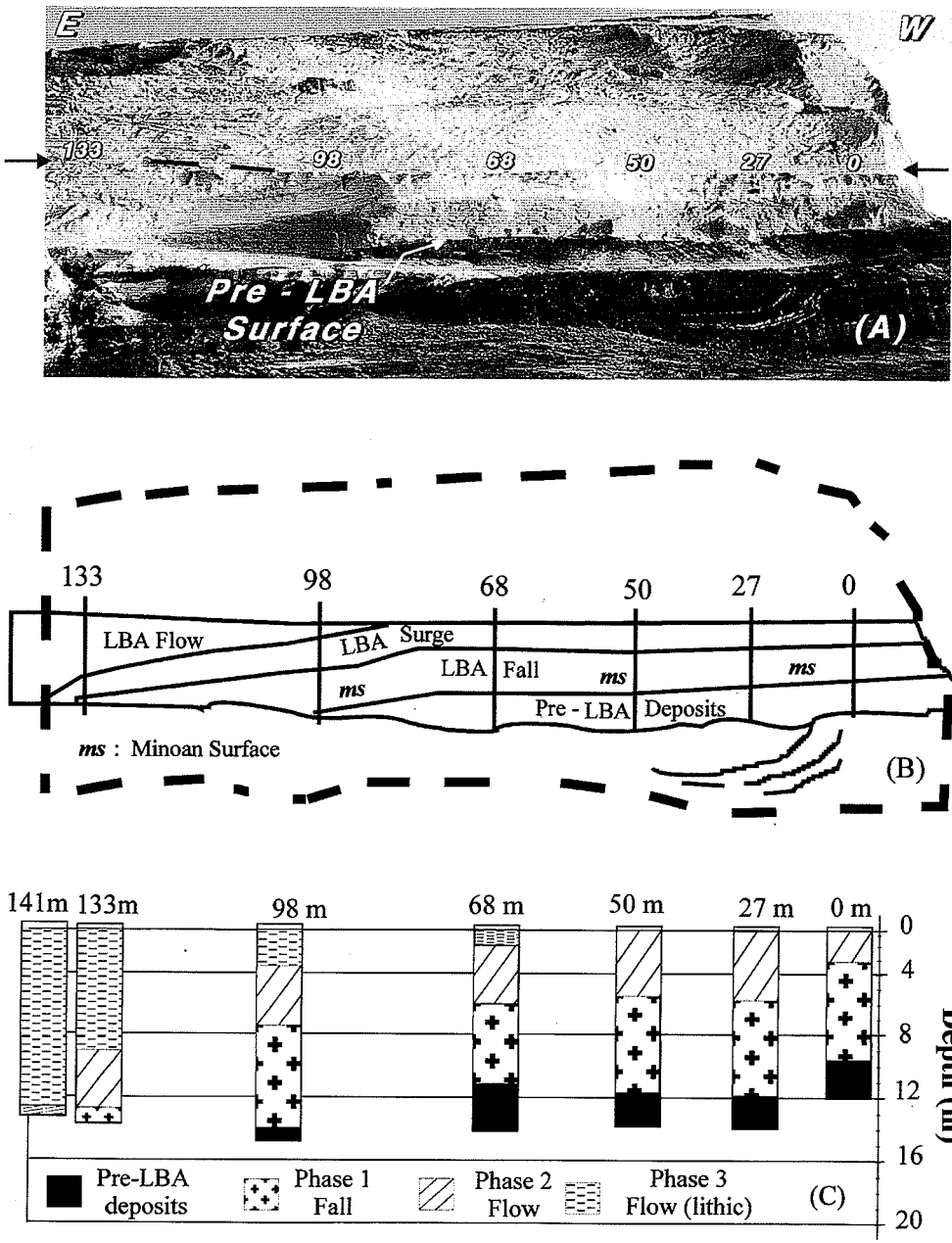

Fig. 2. Volcanic stratigraphy of LBA deposits exposed in Phira quarry. (**a**) Field photograph of quarry bench that was used for 141 m GPR survey. Numbers denote positions of measured stratigraphic columns. (**b**) Schematic cross-section of volcanic stratigraphy shown in field photograph (after Milner 1997). (**c**) Stratigraphic columns for measured sections of LBA volcanic deposits (see text and Fig. 4).

To address this interference we applied a lowpass filter to selectively eliminate the high-frequency noise associated with the background radar signal. Specifically, we chose a cutoff of 10% of the Nyquist frequency or 62.5 MHz and passed only lower-frequency information. All radar data shown in this paper had a lowpass filter applied.

Site A: Phira Quarry

Immediately south of the town of Phira is an abandoned quarry situated on the eastern lip of the caldera. The quarry exposes several hundred metres of Minoan volcanic deposits (Bond & Sparks 1976; Druitt & Francaviglia 1992) lying on top of older volcanic rocks that comprise the ancient Late Bronze Age (Minoan) living surface. The LBA volcanic deposits are all pyroclastic in origin and, in this location, are proximal in nature. We chose to run a GPR survey for calibration purposes along the top of one of the quarry benches (Fig. 2a). Stratigraphic sections were measured at six locations along the front face of the bench. The locations of the sections are marked in each of Fig. 2a, 2b, and 2c. Detailed, and more general, descriptions of these deposits are available from a number of sources (Bond & Sparks 1976; Heiken & McCoy 1984; Druitt *et al.* 1999). The top of the bench is cut into Phase 3 pyroclastic deposits and the survey line is underlain by pyroclastic flow (Phase 3), pyroclastic surge (Phase 2), and fall deposit (Phase 1). The pyroclastic deposits are themselves underlain by well-indurated pre-Minoan volcanic rocks, including a basaltic-andesite lava breccia and well-stratified, finer-grained tuffs.

Figure 2b is a sketch of the field photograph shown in Fig. 2a, and shows the distribution of the individual pyroclastic units in cross-section. The six measured stratigraphic sections are plotted in Fig. 2c. The main features of this stratigraphic section include the following:

(1) the contact between the LBA volcanic deposits and the basement dips slightly to the east and lies between 9 and 14 m beneath the surface of the bench.
(2) Overlying the pre-Minoan volcanic deposits and the Minoan living surface is a well-sorted, massive, 6 m thick fall deposit (Phase 1) comprising pumice lapilli of 1–20 cm. The largest blocks are *c.* 0.2 m. The only structure observable in this unit is a crude coarsening upwards of pumice clasts.
(3) Phase 2 pyroclastic surge is 4–6 m thick, poorly sorted, moderately well laminated, and comprises ash and lapilli with rare block-sized lithic fragments. Laminations dip *c.* 15° to the east and merge asymptotically with the base of the unit. Many layers show prominent cross-laminations.
(4) Phase 3 pyroclastic flow is massive, poorly sorted, and contains large (0.5 m to >2 m) blocks of lithic fragments. Phase 3 contains weak interlayers of pumice beds and has an upper lithic-rich zone. The apparent dip of this crude stratification is *c.* 5–10° east.
(5) As a package, the pyroclastic flow and surge are crudely bedded, form sets of prograding lobes or beds, and dip slightly to the east.

Common-mid-point (CMP) analysis

Two-way travel times are easily converted to depths wherever the velocity of the radar in the deposit is known. The radar velocities or the dielectric properties of these deposits are generally not known *a priori* (e.g. Russell & Stasiuk 1997) and, therefore, an important first task is to estimate the radar velocity of the target deposit. For a well-exposed section, as found in the Phira quarry (Fig. 2a), there are two ways to do so.

A relatively simple way to constrain the velocity is by selecting a range of velocities and finding the one that gives the best 'depth' match between stratigraphic features in the deposit and corresponding reflections in the GPR profile. This method works well where the deposits are homogeneous and contain prominent stratigraphic markers that are also geophysically distinct. In the Phira quarry section, we found that a velocity of 0.1 m ns^{-1} produced a good correspondence between the measured depth to prominent reflectors (e.g. Minoan surface; Fig. 2) and the apparent depth in the radargram (e.g. Fig. 4, see below).

The average radar velocity for these deposits has also been estimated with a field experiment called a CMP survey (Table 1), the results of which are summarized in Fig. 3. Figure 3a shows the GPR data plotted as distance between antennae and energy returned as a function of time. These data are displayed after application of a lowpass filter and with a moderate gain (SEC). Figure 3b shows the results of the CMP analysis in which numerous repeated traces are averaged (stacked) to produce single traces and the results are shown as a function of model velocities (0.01–0.3 m ns^{-1}). The output record is time v. velocity. The appropriate velocity of the deposit is recognized by the trace with the largest

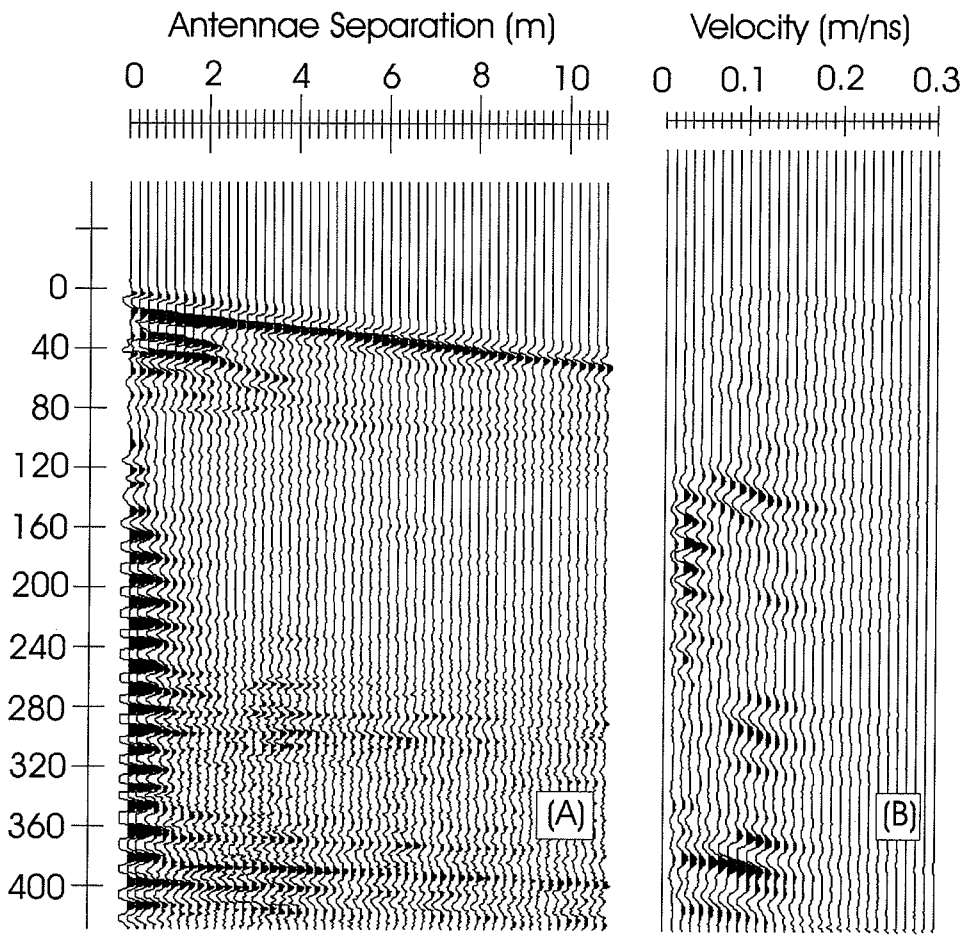

Fig. 3. Results of common-midpoint (CMP) survey run in Phira quarry, used to estimate a value for average radar velocity for LBA volcanic deposits. The CMP data are shown in (**a**) and the analysis of CMP data is plotted in (**b**) (see text).

amplitudes at depth. In this case (ignoring the direct ground- and air-wave data), the velocity appears to be constrained to between 0.09 and 0.11 m ns^{-1}. We elected to use a mean value of 0.1 m ns^{-1} based on this survey, which is consistent with the 'stratigraphic' estimate of average radar velocity.

GPR survey results from Phira quarry

Our survey of LBA volcanic deposits in the Phira quarry was 141 m long, used a 0.5 m sample spacing, and comprised 283 traces. The main purpose of this survey was to calibrate the geophysical results against a well-characterized section of the Minoan pyroclastic deposits.

Figure 4 shows the survey results and compares them with the stratigraphic sections prepared for the face of the quarry bench (e.g. Fig. 2a–c). Figure 4a is a radargram for the survey shown at 2.5 times vertical exaggeration. The radar data are shown after application of a dewow and the lowpass (10%) filter, and have been enhanced with a moderate SEC gain. Figure 4b is a line diagram drawn for the radargram and showing the position and shape of the

Fig. 4. Results of GPR survey of Phira quarry section. (**a**) Radargram (looking south); caldera rim is on the western end of the traverse. (**b**) Line drawing of same section showing prominent reflectors within upper (Phase 2 and 3) pyroclastic flows (bold lines), structures within underlying pre-LBA units (dashed lines labelled B) and a reflection that possibly derives from the quarry wall or other out-of-plane features (R). The shaded region denotes the upper and lower surfaces of the Plinian fall deposit as interpreted from the geophysical data.

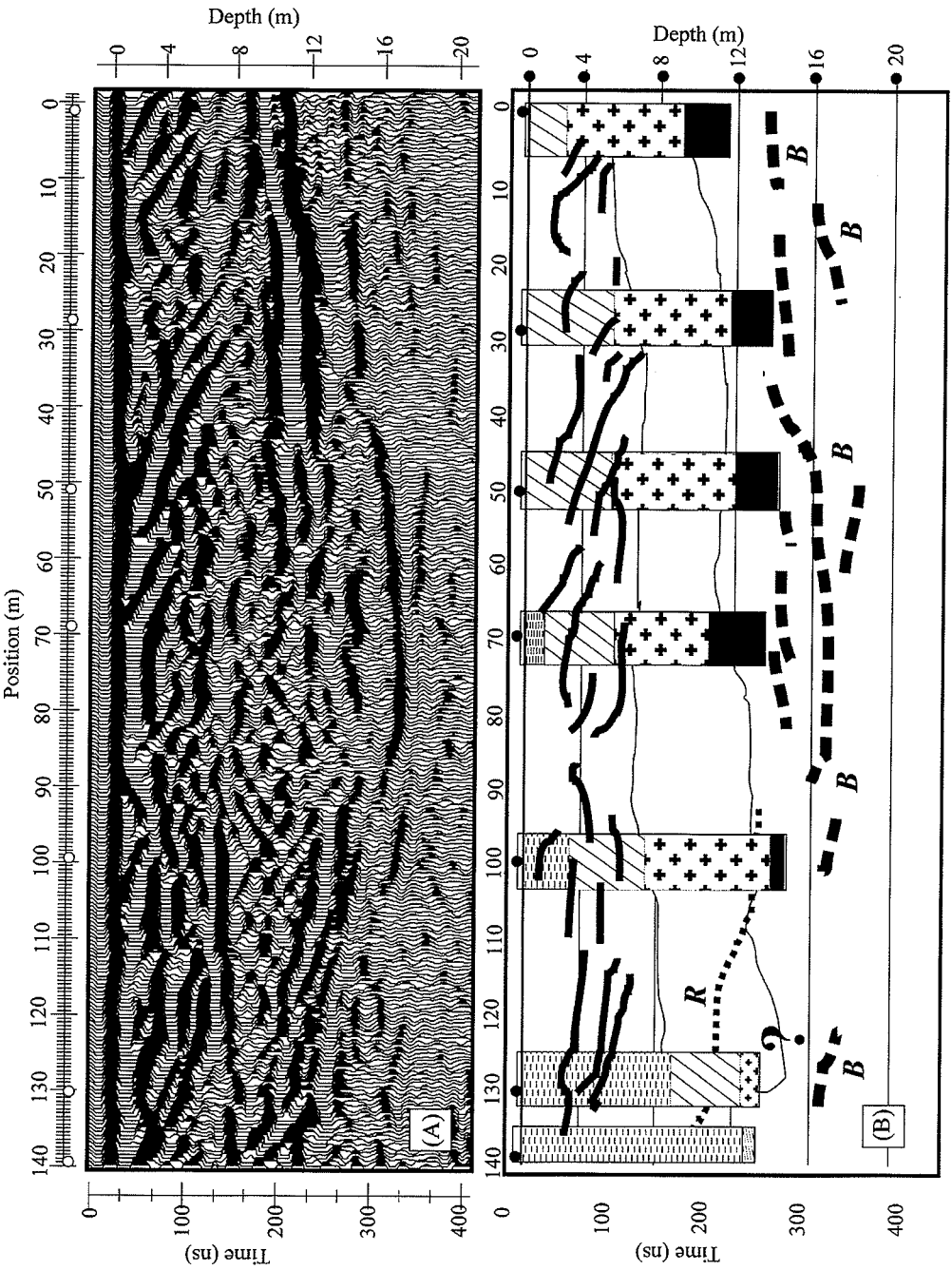
Depth (m)
0
4
8
12
16
20
Position (m)
0
10
20
30
40
50
60
70
80
90
100
110
120
130
140
Time (ns)
0
100
200
300
400
(A)
(B)
B
R
?

prominent geophysical reflectors. Superimposed on the line diagram are lithological columns representing the measured stratigraphic sections as well as a shaded region representing the distribution of the Phase 1 fall deposit as interpreted from the geophysical data.

The radar profile (Fig. 4a) shows information collected for two-way travel times of 0–400 ns; this range corresponds to a maximum depth of just over 20 m ($v = 0.1\ \mathrm{m\ ns^{-1}}$). The radargram shows strong reflectors down to 200–250 ns and weaker, but distinct, reflectors down to 350–400 ns. Furthermore, there is no apparent ringing (echoing of EM waves) at these depths, corroborating our decision to use a 3 m separation. Our interpretation of geological features is based on identifying continuous reflectors or horizons of reflectors that show the same polarity (black v. white). Reflectors that represent the same geological interface should show the same polarity.

There appear to be three distinct packages or regions in the radargram. At times between 200 and 350 ns, the radargram shows a number of continuous but weak reflectors. The reflectors (dashed lines labelled B in Fig. 4b) are variable in attitude: they dip to the east (0–40 m), or are concave upwards (40–100 m), or dip to the west (110–140 m). These are 'basement' reflectors and represent geological structures in the pre-Minoan stratigraphy. The concave-upwards structures are particularly evident in Fig. 2a and b. The signals are weak relative to the more shallow parts of the radargram, but they are constant in character and on this basis are reliable.

The upper portion of the radargram (0–150 ns) also has a very distinctive pattern. This stratigraphic package shows abundant strong discontinuous dipping reflectors (see Fig. 4a and b). The package, taken as a whole, represents the Phase 2 and 3 pyroclastic surge and flow deposits overlying the Phase 1 fall deposit. The most distinctive feature of this part of the radar profile is the abundant choppy, eastward-dipping reflectors seen right across the panel. This feature mirrors the characteristic laminated structure of the surge and flow deposits (Fig. 2a–c).

The last zone shown in Fig. 4a is best displayed between horizontal positions 10 and 110 m and at times of 130 and 190 ns. This part of the radargram is characterized by little or no internal reflection; amplitudes are generally low (little black) and the reflectors that exist tend to be flat and broken-up. The pattern, where viewed from the side, is somewhat reminiscent of cross-hatching. We interpret this zone as indicative of the pyroclastic fall. The fall is homogeneous, massive, and has virtually no internal structure. These properties are consistent with the relatively featureless character of the corresponding portions of the radar section. Our interpretation of the distribution of the Phase 1 fall, based on the radar data, is shown as a shaded region in Fig. 4b. The correlation between our interpretation and the actual distribution (see observed lithological columns) is not perfect but there are pronounced similarities in thickness, dip and position.

Our interpretation of the radargram is somewhat hampered by the presence of a very strong horizontal reflector, which occurs on the eastern end of the traverse at times of 190–210 ns. This reflection, labelled R in Fig. 4b, results from interaction of the EM waves with either the face of the cliff to the quarry bench or the surface of a road located at the base of the cliff-face. The GPR survey was run within a few metres of the face of the bench to optimize the correlations between the radar data and the geological features measured on the face of the quarry bench. The radar beam, however, appears not to be sufficiently focused to avoid generating these artefacts.

Site B: Akrotiri Peninsula

Akrotiri peninsula comprises the southern end of Thera (Fig. 1); at its narrowest the peninsula is just over 1 km in width (Fig. 5). The LBA pyroclastic deposits form a continuous sheet across the peninsula and vertical exposures are more or less limited to the caldera wall or the southern coastline.

We ran a regional-scale GPR survey across the peninsula (Table 1) in two segments as shown in Fig. 5. The traverse is oriented radially to the vent region of the 3600 years BP eruption. The position and orientation of the traverse were chosen so that the survey could sample more proximal deposits near the caldera wall (Fig. 5, no. 1), intersect the Akrotiri archaeological site (Fig. 5, no. 2), and finish at the southern shoreline, where there are more distal pyroclastic deposits (Fig. 5, no. 3).

The primary aim of the regional survey was to map the distribution of LBA volcanic deposits in the subsurface between points of known stratigraphy (Fig. 5, nos 1 and 3). Mapping of young volcanic deposits commonly relies on trust: stratigraphy derived from a few well-exposed sections is used to extrapolate across regions with little or no stratigraphic exposure. Volcanic stratigraphy is notoriously complex, however, and this practice can be very

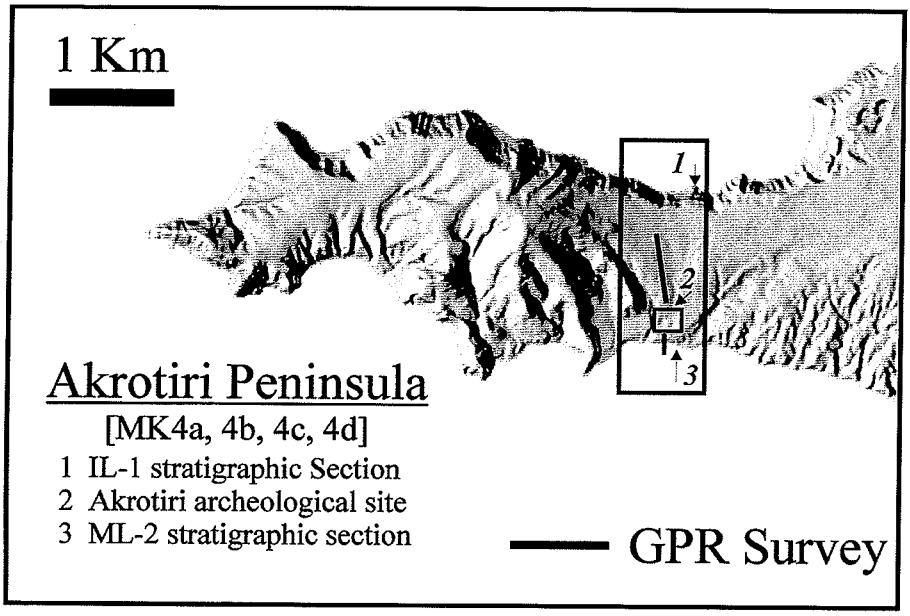

Fig. 5. Detail location map for GPR survey of Akrotiri peninsula showing locations of individual segments of survey line with respect to: (1) stratigraphic section measured on rim of caldera, (2) archaeological excavation site, and (3) stratigraphic column measured on south coast of peninsula.

dangerous without substantial information from areas between sections. Regional-scale GPR surveys can be used to test and strengthen these extrapolations.

In addition to elucidating the distribution of the LBA volcanic deposits, our survey has the ability to define and trace the palaeotopography of the Minoan living surface. In this survey, the results should be of import to researchers working on the Akrotiri excavation site because our results define the thickness of the LBA volcanic deposits and provide physical descriptions of the hinterland to the Minoan townsite. Potentially, the survey can also recover the ancient coastline.

Volcanic stratigraphy of Akrotiri peninsula

Our geophysical survey was constrained at two locations where we measured the stratigraphy of LBA volcanic deposits. We measured a complete section through the LBA deposits exposed in the caldera wall on the northern margin of Akrotiri peninsula. The location of section Il-1 is shown in Fig. 5 (no. 1). Another section (ML-2) was measured on the southern margin of the peninsula just south of the archaeological excavation (Fig. 5, no. 3). The southern section comprises over 30 m of LBA pyroclastic material and clearly represents more distal deposits that were accreted to Thera during the 3600 BP eruption. Both stratigraphic sections are summarized in Fig. 6.

At the caldera wall there are 12 m of LBA volcanic deposits resting unconformably on the pre-Minoan surface. In this location the basement comprises Cape Riva ignimbrite (Druitt 1985; Druitt & Francaviglia 1992). Immediately above the Cape Riva formation is 2 m of Phase 1 fall deposit. Phase 2 surge overlies the fall; it is strongly laminated and contains abundant red-oxidized lapilli. The upper 7 m of the section is made of poorly laminated Phase 3 pyroclastic flow (*c.* 5 m) capped by just over 2 m of Phase 4 ignimbrite. The Phase 4 ignimbrite comprises a tan-coloured ash matrix containing abundant lithic fragments. The unit shows a crude stratification defined by concentrations of block-sized dense lava lithic fragments. The concentrations of lithic fragments form discrete horizons, which show substantial topography and are commonly channel-like in form. The top of the section is more or less even in elevation with the north end of the GPR traverse (e.g. MK4D, Table 1).

The stratigraphic sequence measured at the southern coastline (ML-2; Fig. 6) is substantially different. There is a depth of over 30 m of exposed LBA volcanic deposits and, although the section is continuous to sea level, the

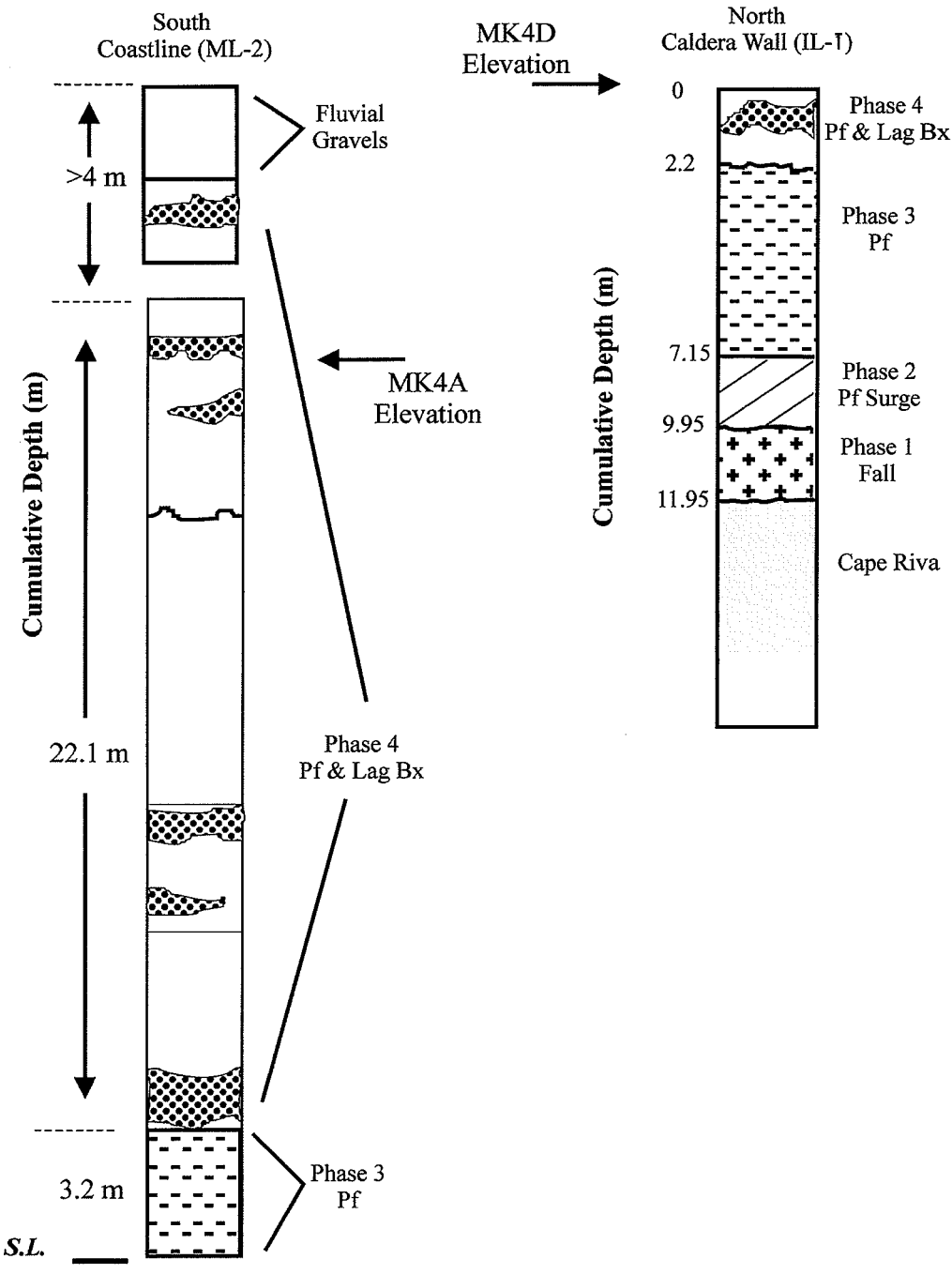

Fig. 6. A comparison of LBA volcanic stratigraphy measured for the northern edge of the Akrotiri peninsula and situated on the south rim of the caldera (no. 1: Fig. 5), and for the southern shoreline of the Akrotiri peninsula and immediately south of the archaeological excavation site (no. 3: Fig. 5). Sections compare thicknesses of pyroclastic fall and flow (Pf) deposits and show distribution of lag breccias (Bx).

pre-Minoan surface is not exposed. Phase 1 and 2 deposits are absent from the section. The base of the section is made up of slightly over 3 m of Phase 3 pyroclastic flow; the unit is massive and made up of lithic and pumice lapilli in a fine-grained ash matrix. Overlying Phase 3 and making up most of the section (>24 m) is Phase 4 ignimbrite. The majority of the unit is massive, fine-grained, poorly sorted material with lenses and lithic-rich layers or domains. These layers mainly comprise dense lava clasts, which range in size from lapilli to blocks. The layers can be continuous and define a slight (<2°) dip towards the coast. Conversely, they can occur as discontinuous and trough-shaped lenses. The layers vary from centimetre scale to several metres in thickness. Finer-grained lithic lenses sometimes are graded.

In the region of the Akrotiri archaeological site, Phase 4 deposits are capped by fluvial gravel and boulder deposits. These deposits are generally erosive into the Phase 4 ignimbrite and form discontinuous channels or sheets. At this locale (ML-2) there are between 2 and 4 m of this deposit sitting on top of Phase 4. Also shown in Fig. 6 is the elevation of the GPR traverse (MK4A) relative to the stratigraphic column. The southern end of our GPR survey ends at an elevation below the flash flood gravel deposits.

GPR results from Akrotiri peninsula

Our survey across the Akrotiri peninsula was completed in two segments: a northern segment that ran south from a point near the caldera wall towards the northern edge of the Akrotiri excavation site, and a short segment that extended from the southern boundary of the same excavation site towards the coast (Fig. 5). The survey was over 0.5 km long and used a 1.0 m sample spacing (Table 1). The survey results are shown in two separate radargrams at *c.* 2X vertical exaggeration (Figs 7 and 8).

Figure 7 shows the survey results for the northern 552 m segment from the caldera side of the peninsula (N) to the edge of the Akrotiri excavation (S). The three panels are continuous, and oriented as if the viewer is looking westward, and are best read from right (N) to left (S).

The radar data reveal a simple consistent stratigraphy for the first 350 m of the traverse (upper & middle panels, Fig. 7). Again, the radargram for 0–350 m can be broken down into three packages on the basis of their distinctive geophysical character. In the middle of the section between 100 and 200 ns (4.5–9 m) there is a zone of low-amplitude signal (featureless grey). The lower half of the section between 200 and 400 ns is characterized by weaker, discontinuous reflectors overprinted by occasional stronger, concave-down reflectors. The upper portion of the radargram between 0 and 100 ns shows a third distinctive pattern characterized by strong reflections.

The radar data from the distinctive low-amplitude zone suggest a deposit that is uniform in thickness (2–3 m), continuous, and homogeneous without internal structure (e.g. no internal reflectors). We interpret this zone (Fig. 7; P_1) as corresponding to the Phase 1 fall; the lower contact is against the pre-Minoan surface of Cape Riva ignimbrite (Fig. 7; CR) and the upper contact is with Phase 2 and 3 LBA pyroclastic deposits (Fig. 7; $P_{2,3,4}$). The upper contact is marked by a prominent, flat-lying, and more or less continuous reflector at 4.0–5.5 m depth, which maintains its polarity across the radargram; this is evident from the consistent red–blue–red striping. The lower contact between LBA fall and Cape Riva ignimbrite is marked by a set of weaker, flat-lying, somewhat discontinuous reflectors at about 9 m depth. The fact that the polarity and orientation of these reflections is also maintained across the section is strong support for our interpretation.

The radar data from 200 ns and below represent structure within the pre-Minoan basement. Most reflectors are weak and horizontal; however, between 200 and 340 m several deeper (12–16 m) and more continuous curving reflectors appear in the unmigrated data.

The upper 100 ns of the radargram comprises strong, continuous and segmented, horizontal reflectors, which are interwoven with strong, discontinuous, southward-dipping reflectors. The data are consistent with a series of strongly layered deposits, which are locally cross-laminated or have abundant internal structure. We interpret these as LBA pyroclastic surge and flow units (e.g. Phases 2–4) sitting on top of the Phase 1 fall deposit. In particular, the dipping structures seen at positions 133 m, 150 m, 230 m, and between 270 and 330 m are entirely consistent with the overall lobate structure of these pyroclastic deposits and their strong internal structure (see Fig. 6).

The lower panel shows survey results from immediately north of the excavation site. Electromagnetic interference from a metal fence can be seen in traces from the last 5 m of the survey (Fig. 7; F). The radar data in the lower panel show the same stratigraphic packages but with some important differences. First, the contact between the Phase 1 fall and the Cape Riva

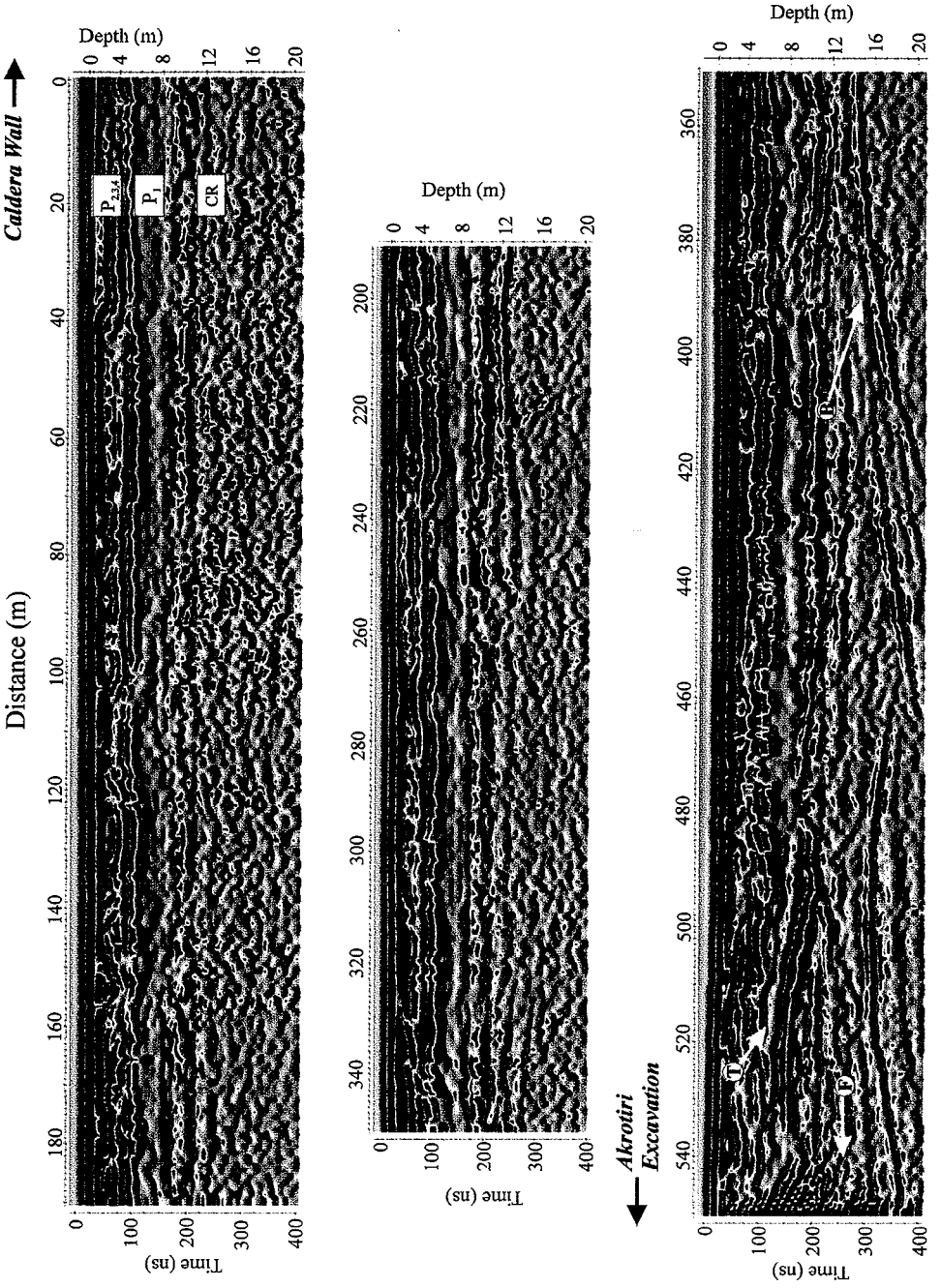
Caldera Wall
Distance (m)
Depth (m)
Time (ns)
$P_{2,3,4}$
P_1
CR
Akrotiri
Excavation
A
B
C

ignimbrite begins at about 9–10 m depth but shallows substantially to the south as the basement rises. This rise is the first topographic irregularity seen on the pre-Minoan surface over this traverse (Fig. 7; T); to this point the topography has been uniformly shallow dipping and flat. Attending this rise in topography is a distinctive thinning of the Phase 1 fall deposit relative to the flats. The upper package of pyroclastic flows (0–100 ns) has a character consistent with that observed in the other two panels and it also appears to thin over the basement high.

A second difference is seen in the lower half of the radargram. Many more continuous reflectors are seen within the pre-Minoan rocks (Fig. 7; B). Indeed, there are prominent structures seen at depths of 20–22 m. The continuous concave-downwards reflectors seen in the unmigrated section may represent the edges of small cliffs or steps in the basement topography.

In summary, the northern segment of this GPR survey establishes several important elements. First, we are clearly able to see the interface between the LBA volcanic deposits and the Minoan living surface as represented by the Cape Riva ignimbrite. Second, we can identify the Phase 1 fall deposit based on its geophysical character. Because of its unique character, it is possible to trace the fall deposit in the subsurface for the full length of this segment of the survey. The unit is between 2 and 3 m thick and clearly mantles the underlying topography. The fall appears to be of uniform thickness and character except where it mantles a relative high in the palaeotopography. Third, the fall is capped by LBA pyroclastic surge and flow (Phases 2–4). These units are more or less constant in thickness (*c.* 5 m), although there is a hint that the total package thickens very slightly from north to south from 4.5 to 6 m respectively. In some instances our survey elucidates structures as deep as 20–22 m.

The southern segment of the traverse across the Akrotiri peninsula is 30 m long and begins on the southern edge of the archaeological excavation site. Figure 8 shows radar results for this segment of the traverse (left panel) and, for comparison, repeats (right panel) the radar data for the last 90 m of the traverse shown in Fig. 7. The two radar panels are shown at the same scale and vertical exaggeration, although longer listening times (Table 1) were used for the southern leg, to image deeper structures. The interval between the two panels represents the fenced area (400–450 m) of the archeological site.

Within the radargram for the southern segment (Fig. 8; left panel) is a single 'non-geological' reflection; the artefact is an EM reflection from an overhead powerline situated a short distance south of the end of the section (Fig. 8; A). This reflection is manifested in the radargram by the apparent reflecting interface dipping to the north with a characteristic slope corresponding to the speed of light in air (0.3 m ns^{-1}) at depths of 16–24 m (Fig. 8). The remaining reflectors (all south dipping or flat) are interpreted as geological features in the subsurface.

The subsurface structure for the southern segment is distinct from that found for the northern part of the traverse (Fig. 7; Fig. 8, right panel). First, the Phase 1 fall unit, characterized by a continuous, mantling zone of low amplitudes is absent. Second, there is no clear evidence of an interface that could be interpreted as the Minoan living surface. Furthermore, the interfaces that can be seen define a package of deposits dipping southward with dips shallowing with decreasing depth. In the near surface (top 6 m) the structures are similar in both parts of the survey (compare the left and right panels, Fig. 8).

The southern portion of the survey is short and our coverage in this area somewhat sparse, hence only a preliminary interpretation is offered here. Our interpretation relies heavily on geological observations made at the coastal cliffs 50–60 m south of the endpoint of the GPR survey. The stratigraphic section (ML-2) for the south coast (Fig. 6) is repeated in Fig. 8, and has been positioned to reflect its proper elevation relative to the GPR survey. At this location on the coast, Cape Riva ignimbrite is not exposed and neither is the Phase 1 fall, nor Phase 2 surge deposits. Phase 3 and 4 pyroclastic flow deposits are thicker than at more proximal locations (e.g. IL-1; Figs 5 and 6), having a total combined exposed thickness of about 25 m. It is evident from this and other distal locations on the coast that the pyroclastic flow deposits have considerably extended the coastline of the island.

Fig 7. Radargrams for the northern portion of the GPR survey across the Akrotiri peninsula with the viewer looking west. The 552 m traverse from the caldera side of the peninsula (N) to the edge of the Akrotiri excavation (S) is portrayed as three panels, each of which should be read continuously and from right (N) to left (S). Symbols in upper panel denote Cape Riva (CR) basement overlain by Phase 1 fall (P_1) and a combination of Phase 2, 3 and 4 deposits ($P_{2,3,4}$). Symbols in lower panel illustrate prominent reflector in basement (B), thinning of Phase 1 as a result of topographic rise (T), and interference because of metal fence enclosing the Akrotiri site (F).

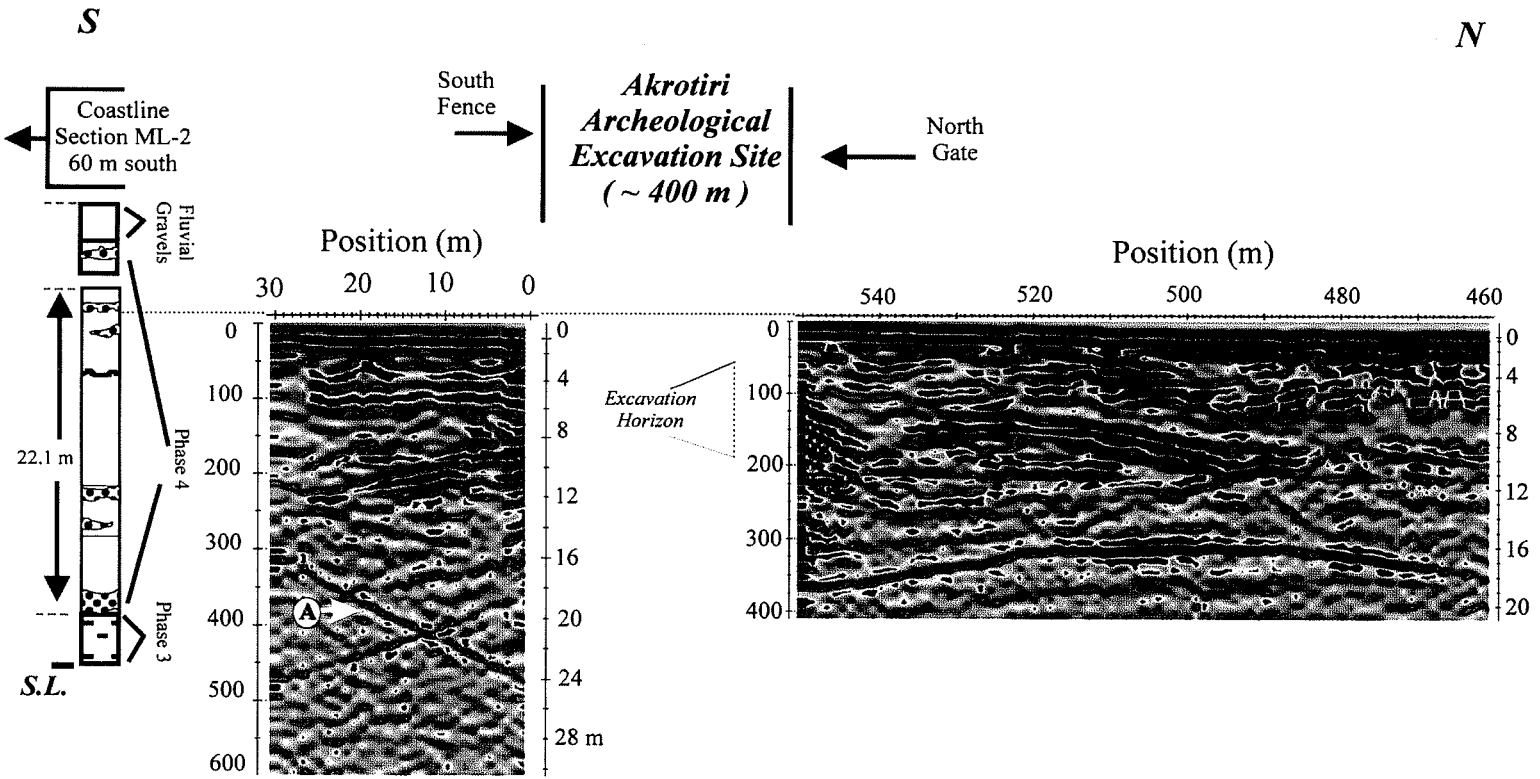

Fig. 8. Radar results for the southern termination of the traverse across the Akrotiri peninsula. The segment is 30 m long and ends against the southern edge of the Akrotiri archaeological excavation site (left panel). The radar data for the last 90 m of the traverse shown in Fig. 7 are repeated for comparison. The interval between the two panels represents the fenced area of the archaeological site. Symbol (A) indicates a non-geological reflection because of above-ground powerline (see text).

We would argue, on the basis of the GPR data shown in Fig. 8 (left panel) and the geological observations summarized in Fig. 6 (ML-2), that the Minoan shoreline was situated somewhere between the southern leg of our survey (MK4a) and the current ancient Akrotiri excavation site. The deposits that we have imaged south of the excavation site represent, in our opinion, a pyroclastic apron extending into the Late Bronze Age sea. The signal character, depth and upward-shallowing dips shown in the radargram (Fig. 8; left panel) are consistent with the internal structure of a prograding pyroclastic apron (Jol & Smith 1991) formed from numerous flow units or pulses of pyroclastic flows. Notably, at times below 420 ns there is an absence of reflectors; this depth corresponds to sea level and is the probable location of the local water table.

If the location of the southern leg of the GPR survey is at a position that was offshore before the LBA eruption, can we also infer the nature of this portion of the LBA coastline? The total thickness of these deposits (>25 m), combined with their proximity to the partially excavated Minoan settlement (which establishes a relative elevation for the Minoan living surface), suggests a significant elevation drop (20–30 m) over a narrow horizontal distance (<50–75 m). We imagine that the Minoan living surface must have dropped away to the sea very rapidly from the southern limit of the settlement, and suggest that this part of the settlement was built out onto sea cliffs that were situated slightly north of the left panel in Fig. 8. This argues for the presence of a bay or harbour serving the ancient town, which must have been located east or west of the survey section. It is clear that further work is needed to establish the exact nature of this portion of the ancient Minoan coastline, and that GPR could be fruitfully used for this purpose.

Conclusions

The results of our GPR surveys of LBA pyroclastic deposits on Thera indicate that GPR can consistently image LBA deposits to depths of 15 m and can return information on reflectors at depths of 20–25 m. The method can distinguish between the LBA deposits and the underlying Minoan living surface, as well as distinguish between different types of pyroclastic deposits such as air fall vs. pyroclastic flow.

The consequences of these points are as follows. First, the distributions and thicknesses of the different components of the LBA deposits can be traced across the island. This has implications for understanding both the volcanic history of the island (e.g. Bond & Sparks 1976; Druitt 1990; Doumas *et al.* 1997), the destruction of the island (Sparks 1979; Sigurdsson *et al.* 1990; McCoy & Heiken 1994) and nature of the pre-eruption surface (e.g. Rackham 1990; Forsyth 1996; Friedrich *et al.* 2000). For example, the area immediately north of the ancient Akrotiri townsite is underlain by a uniform 10–12 m blanket of LBA deposits including pyroclastic fall, surge and flow deposits. The stratigraphic package changes profoundly in nature immediately south of the town site.

Second, the interface between the LBA volcanic deposits and the Minoan living surface can be defined and traced even where not exposed, allowing mapping of the palaeotopography (e.g. Heiken *et al.* 1990; Druitt & Francaviglia 1992; Forsyth 1996). For example, our survey shows that immediately north of the Akrotiri town site lay flat, probably uninhabited land which would have been appropriate for agriculture (e.g. Rackham 1990), and that the town site was probably built out onto sea cliffs. Furthermore, although our surveys did not uncover any direct evidence in the subsurface of man-made structures, these data suggest that future regional surveys could identify walls and buildings belonging to the Minoan civilization.

Funding for this research derives from a number of sources. Purchase of the PulseEKKO 100 instrument from Sensors and Software was made possible through an NSERC–Industry partnership grant between the University of British Columbia and Golders Associates. We are indebted to M. Maxwell and J. Schmok for this partnership and for their technical advice. Operational funds for the fieldwork came from NSERC Research Grant A0820 (J.K.R.) and from the University of Toronto (M.V.S.). We are indebted to T. Druitt for his introduction to the geology and volcanology of Thera, and for his critical analysis of results from our field surveys. We also were aided by the efforts and support of G. Vougioukalakis from the Institute of Geology and Mineral Exploration. Lastly, our fieldwork was greatly facilitated with the assistance of P. L. Cowlishaw, L. Stasiuk and L. Zeppos.

References

AITKEN, M. J. 1988. The Thera eruption: continuing discussion of the dating. *Archaeometry*, **30**, 165–182.

ANNAN, A. P. & DAVIS, J. L. 1977. *Radar Range Analysis for Geological Materials*. Geological Survey of Canada, Paper, **77–1B**, 117–124.

ARDON, O. F. P. 1985. Comparison among seismic refraction, electrical resistivity and ground probing radar methods for shallow underground

structure investigation. *Individual Studies by Participants at the International Institute of Seismology and Earthquake Engineering*, **21**, 83–98.

BOND, A. & SPARKS, R. S. J. 1976. The Minoan eruption of Santorini, Greece. *Journal of the Geological Society, London*, **132**, 1–16.

CAMERLYNCK, C., DABAS, M. & PANISSOD, C. 1994. Comparison between GPR and four electromagnetic methods for stone features characterization: an example. *Archaeological Prospection*, **1**, 5–17.

CLARKE, K. C. & CROSS, G. M. 1989. Radar imaging of glaciovolcanic stratigraphy, Mount Wrangell caldera, Alaska: interpretation, model and results. *Journal of Geophysical Research*, **94**, 7237–7249.

DAVIS, J. L. & ANNAN, A. P. 1989. Ground-penetrating radar for high-resolution mapping of soil and rock stratigraphy. *Geophysical Prospecting*, **37**, 531–551.

DOUMAS, C., GURIOLI, L., SBRANA, A. & VOUGIOUKALAKIS, G. 1997. Stratigraphy of the 1628 BC (Minoan) Plinian deposits in the Akrotiri settlement: inferences on precursory phenomena and eruptive scenario of the Minoan event and comparisons with Pompeii and Ercolano archeological settlements. *In*: *Volcanoes, Earthquakes and Archaeology*, Volcanic & Magmatic Studies Meeting, April 1997, 17.

DRUITT, T. H. 1985. Vent evolution and lag breccia formation during the Cape Riva eruption of Santorini, Greece. *Journal of Geology*, **93**, 439–454.

——1990. The pyroclastic stratigraphy and volcanology of Santorini. *In*: HARDY, D. A. (ed.) *Thera and the Aegean World III, Vol. 2*. Thera Foundation, London, 27–28.

—— & FRANCAVIGLIA, V. 1992. Caldera formation on Santorini and the physiography of the islands in the Late Bronze Age. *Bulletin of Volcanology*, **54**, 484–493.

——, EDWARDS, L., MELLORS, R. M., PYLE, D. M., SPARKS, R. S. J., LANPHERE, M., DAVIES, M. S. & BARREIRIO, B. 1999. *Santorini Volcano*. The Geological Society, London, Memoir, **19**.

FORSYTH, P. Y. 1996. The pre-eruption shape of Bronze Age Thera: a new model. *Ancient History Bulletin*, **10.1**, 1–10.

FRIEDRICH, W. L., SEIDENKRANTZ, M.-S. & NIELSEN, O. B. 2000. Santorini (Greece) before the Minoan eruption; a reconstruction of the ring-island, natural resources and clay deposits from the Akrotiri excavation. *This volume*.

FYTIKAS, M., KOLIOS, N. & VOUGIOUKALAKIS, G. 1990. Post-Minoan volcanic activity of the Santorini volcano. Volcanic hazard and risk, forecasting possibilities. *In*: HARDY, D. A. (ed.) *Thera and the Aegean World III, Vol. 2*. Thera Foundation, London, 241–249.

GILBERT, J. S., STASIUK, M. V., LANE, S. J., ADAM, C. R., MURPHY, M. D., SPARKS, R. S. J. & NARANJO, J. A. 1996. Non-explosive, constructional evolution of the ice-filled caldera at Volcan Sollipulli, Chile. *Bulletin of Volcanology*, **58**, 67–83.

GOODMAN, D. 1994. Ground-penetrating radar simulation in engineering and archeology. *Geophysics*, **59**, 224–232

HEIKEN, G. & MCCOY, F. 1984. Caldera development during the Minoan eruption, Thira, Cyclades, Greece. *Journal of Geophysical Research*, **89**, 8441–8462.

——, —— & SHERIDAN, M. 1990. Palaeotopographic and palaeogeologic reconstruction of Minan Thera. *In*: HARDY, D. A. (ed.) *Thera and the Aegean World III, Vol. 2*. Thera Foundation, London, 370–376.

HOLLOWAY, A. L., SOONAWALA, N. M. & COLLETT, L. S. 1986. Three-dimensional fracture mapping in granite excavations using ground-penetrating radar. *Canadian Institute of Mining Bulletin*, **79**, 54–59.

JOL, H. M. & SMITH, D. G. 1991. Ground penetrating radar of northern lacustrine deltas. *Canadian Journal of Earth Sciences*, **28**, 1939–1947.

—— & ——1992. *Geometry and Structure of Deltas in Large Lakes: a Ground-Penetrating Radar Overview*. Geological Survey Finland, Special Paper, **16**, 159–168.

KNOLL, M. D., HAENI, F. P. & KNIGHT, R. J. 1991. *Characterization of a sand and gravel aquifer using ground-penetrating radar, Cape Cod, Massachusetts*. US Geological Survey, Water Resources, Investigation Report **91-4034**, 29–35.

LINER, C. L. & LINER, J. L. 1995. Ground-penetrating radar: a near-face experience from Washington County, Arkansas. *Leading Edge*, **18**, 17–21.

MARCO, S., AGNON, A., ELLENBLUM, R., EIDELMAN, A., BASSON, U. & BOAS, A. 1997. 817-year-old walls offset sinistrally 2.1 m by the Dead Sea transform, Israel. *Journal of Geodynamics*, **24**, 11–20.

MARINATOS, S. 1939. The volcanic destruction of Minoan Crete. *Antiquity*, **13**, 425–439.

MCCOY, F. W. & HEIKEN, G. 1994. The Minoan eruption; a Late Bronze Age volcanic disaster in Greece. *Geological Society of America, 1994 Annual Meeting, Abstracts with Programs*, **26**, 263.

——, PAPMARINOPOULOS, S., DOUMAS, C. & PALYVOU, C. 1992. Probing the Minoan eruption on Thera with ground-penetrating radar: buried extent of Akrotiri, tephra stratigraphy and late-Bronze Age volcanic hazards. *Geological Society of America, 1992 Annual Meeting, Abstracts with Programs*, **24**, 26.

MILNER, W. 1997. *Forward modelling GPR response over dry volcanic facies: testing the suitability of GPR mapping at Santorini volcano*. BASc thesis, University of British Columbia, Vancouver.

PRATT, B. R. & MIALL, A. D. 1993. Anatomy of a bioclastic grainstone megashoal (Middle Silurian, southern Ontario. revealed by ground-penetrating radar. *Geology*, **21**, 223–226

RACKHAM, O. 1990. Observations on the historical ecology of Santorini. *In*: HARDY, D. A. (ed.) *Thera and the Aegean World III, Vol. 2*. Thera Foundation, London, 384–391.

REA, J., KNIGHT, R. & RICKETTS, B. D. 1994. Ground-Penetration Radar Survey of the Brookswood Aquifer, Fraser Valley, British Columbia. *Current Research*, Geological Survey of Canada, **1994-A**, 211–216.

RUSSELL, J. K. & STASIUK, M. V. 1997. Characterization of volcanic deposits with ground penetrating radar. *Bulletin of Volcanology*, **58**, 515–527.

——, SCHMOK, J., NICHOLLS, J. *et al.* 1998. The Ice Cap of Hoodoo Mountain Volcano, Northwestern British Columbia: Estimates of Shape and Thickness from Surface Radar Surveys. Geological Survey of Canada, *Current Research*, **1998-A**, 55–63.

SMITH, D. G. & JOL, H. M. 1992. Ground-penetrating radar investigation of a Lake Bonneville delta, Provo level, Brigham City, Utah. *Geology*, **20**, 1083–1086.

SIGURDSSON, H., CAREY, S. & DEVINE, J. D. 1990. Assessment of the mass, dynamics and environmental effects of the Minoan eruption of Santorini volcano. *In*: HARDY, D. A. (ed.) *Thera and the Aegean World III, Vol. 2.* Thera Foundation, London, 100–112.

SPARKS, R. S. J. 1979. The Santorini eruption and its consequences. *Endeavor, New Series*, **3-1**, 27–31.

STASIUK, M. V. & RUSSELL, J. K. 1994. Preliminary Studies of Recent Volcanic Deposits in Southwestern British Columbia using Ground Penetrating Radar. *Current Research*, Geological Survey of Canada, **1994-A**, 151–157.

VAUGHAN, C. J. 1986. Ground-penetrating radar survey used in archeological investigations. *Geophysics*, **51**, 595–604.

WILLIAMS, H. & CRONKITE-PRICE, S. M. 1995. Excavations at Stymphalos 1994. *Echos du Monde Classique – Classical Views*, **XXXIX** (n.s. 14), 1–22.